Experimental and numerical study of section restriction effects on filling behavior in aluminum low-pressure casting

A. SANITAS[1], M. BEDEL[1] and M. EL MANSORI[1]

[1] *MSMP Laboratory (EA-7350), Arts et Metiers ParisTech, 2 cours des Arts et Metiers, 13617 Aix en Provence, France*

[a]antonin.sanitas@ensam.eu, [b]marie.bedel@ensam.eu, [c]mohamed.elmansori@ensam.eu

Abstract

The effect of pressurizing speed and mold geometry on mold filling in aluminum low-pressure casting was studied. The filling of cylindrical sand molds was both experimentally measured and simulated to characterize the free surface front velocity as linked to the mold geometry. Cylindrical molds with different diameters were filled with liquid $AlSi_{13}$ alloy. The mold filling velocity was experimentally measured using electrical contacts and was simulated using ANSYS Fluent® simulation software. The experimental results show that during mold filling without any section change, the filling velocity is regular and follows the Bernoulli's equations. However, adding a sudden section restriction in the mold leads to oscillating filling phenomena. Moreover, the oscillation intensity is observed to be proportional to the imposed filling pressure ramp. These oscillations lead to a temporary increased velocity of the metal front, which could induce metal oxidization and reduced mechanical properties for the cast part. The presented fluid dynamics simulation results show the importance of simulating the tube and not only the mold to catch the dynamic effects of the process on filling. Simulating the tube or the whole system, the observed filling oscillations are quantitatively predicted by the model. An analytical model is proposed to forecast the effect of the restriction function of geometry and pressure ramp. It permits to define new guidelines for low pressure casting part designs and the associated process adjustments.

Keywords: low pressure casting, aluminum alloys, mold filling, fluid flow oscillations

Nomenclature

$\dot{P_f}$	Pressure ramp	$Pa.s^{-1}$
S_c	Mold cavity horizontal cross section	m^2
S_f	Furnace horizontal cross section	m^2
S_t	Tube horizontal cross section	m^2
h_m	Mold cavity height before section change	m
h_{tube}	Tube height	m
h_t	Total height ($h_m + h_{tube}$) of diameter ϕi_{tube}	m
ϕ_c	Mold cavity diameter	m
ϕ_f	Furnace diameter	m
ϕi_{tube}	Tube internal diameter	m
ϕe_{tube}	Tube external diameter	m
P_f	Furnace air pressure	Pa
P_a	Atmospheric air pressure	Pa
P_m	Metal pressure at the interface between tube and mold	Pa
R	Section restriction factor in the mold cavity (S_c/S_t)	$-$
ρ	Alloy density	$kg.m^{-3}$
g	Standard gravity	$m.s^{-2}$
α	Section restriction factor between tube and furnace (S_t/S_f)	$-$
v_t	Melt velocity in the tube	$m.s^{-1}$

v_c	Melt velocity in the mold cavity	$m.s^{-1}$

1. Introduction

In gravity casting, as in Low Pressure Casting (LPC), the first step in making a part free of defect is to fill the mold properly. The filling optimization objective is to reduce the metal velocity to a minimum value without inducing misrun (Edler et al., 2006). Indeed, on one hand, a too high velocity would induce a turbulent filling flow, leading to the risk of generating oxides in the parts. On the other hand, a too low velocity would lead to early solidification and therefore an incomplete filled part.

To determine the upper limit velocity in the system, a common criterion was proposed by Campbell, independent of the local geometry (Campbell, 2003). By analyzing the relationship between filling velocity of the metal front, melt density and surface tension, this criterion gives an upper limit velocity of 0.5 m/s for aluminum alloys. Experimental aluminum gravity casting (Runyoro et al., 1992) and LPC casting both for industrial part (Puga et al., 2016) and for a simple plate geometry (Liu et al., 2015) confirmed that above this critical value, the mechanical properties of the parts are reduced due to oxides entrapment.

To identify the lower limit of filling velocity, coupled thermal, hydraulic and solidification mechanisms responsible for misrun were studied, mainly in gravity casting. Different models were developed to link casted length and casting properties, for different alloys. The most simple model links proportionally an empirically determined freezing time to the metal filling velocity (Campbell, 2003). More developed energetic models (Flemings et al., 1961) or hydraulic models (Luk and Darvell, 1992) also directly link casted length and metal velocity. The importance of filling velocity on misrun was experimentally confirmed in aluminum gravity castings (Flemings, 1964) but also in aluminum composite LPC (Konopka et al., 2015) and magnesium alloy LPC for plates (Sadayappan et al., 2006), bars (Laws et al., 2006) or tubes (Sanitas et al., 2017). Moreover, the filling time in LPC has a great influence on grain size and final mechanical properties (Fu et al., 2008). Therefore, the velocity mastering during filling is clearly a key factor influencing the final cast part quality.

In gravity casting, the liquid metal velocity is mainly dependent on the metallostatic pressure evolution during mold filling, which is related to the mold design (Campbell, 2003). On the opposite, in low pressure casting, the liquid metal velocity is induced not only by the mold design but also by the filling pressure ramp (Edler et al., 2006). This additional processing parameter should allow the control of the fluid flow without modifying the mold geometry. Indeed, in low pressure casting, the pressure of the gas above the liquid metal is gradually increased in the furnace. The metallostatic head pressure of the metal is hence compensated and the metal is forced to rise through the rising tube towards the mold.

To choose the adapted pressure ramp, numerical simulation is a precious tool. In previous numerical works, different system geometries were considered; when the whole LPC furnace is taken into account in some models (Puga et al., 2016), only the rising tube and the mold (Liu et al., 2015) or even only the mold (Kuo et al., 2001) are considered in other works. In the last case, the pressurizing gas and the liquid metal in the furnace are not considered but replaced by a boundary condition at the riser tube - mold interface, resulting in calculation time savings. The pressure at the riser tube -

mold interface was analytically linked to the gas pressure in the furnace. Assuming that the dynamic pressure of the fluid is negligible, the flow is laminar, the fluid density is constant and the evolution of the metal level in the furnace during filling is negligible, the relationship between the gas pressure P_f , the metal pressure at the tube - mold interface P_m and the rising tube height h_{tube} can be expressed (Duff, 1995):

$$P_f - \rho g h_{tube} = P_m \qquad \text{(Eq-1)}$$

The hypothesis of a steady state with perfect linear increase of gas pressure in the furnace has implicitly been made. Other works directly used analytical equations to link rising metal velocity to gas pressure ramp using the same assumptions. Considering $\dot{P}_f$ as the derivative of the gas pressure in $Pa.s^{-1}$, the Eq-2 gives the vertical filling velocity V_z (Hogg et al., 1991).

$$V_z = \frac{\dot{P}_f}{\rho g} \qquad \text{(Eq-2)}$$

However, in this very simple model, furnace and mold geometries are neglected. Liu et al. added in this analytical equation the influence of horizontal furnace and mold cavity cross sections (Liu et al., 2015). Defining S_c, S_t and S_f respectively as filled mold cavity, rising tube and furnace horizontal cross sections, Eq-3 links $\dot{P}_f$ the pressure ramp in $Pa.s^{-1}$; ρ the alloy mean density in $kg.m^{-3}$; $g = 9.81 m.s^{-2}$ and v_t the mean velocity in the tube in $m.s^{-1}$:

$$\dot{P}_f = \rho g \left(1 + \frac{Sc}{Sf}\right) \frac{St}{Sc} v_t \quad \text{(Eq-3)}$$

Those analytical equations can then be compared to experimental studies. Liu et al. (Liu et al., 2015) studied the effect of different pressure ramps on the metal front filling behavior for a sudden section increase between tube and part (by a factor 20). Simulating the tube and mold geometries, they revealed that a section change induces oscillations that increase in amplitude when increasing the pressure ramp. Fan et al. (Fan and Ji, 2005) used similar hydrodynamics hypothesis to estimate the filling velocity in low pressure casting of a lost foam mold with sudden section reduction by a factor 0.76. The comparison showed a good correlation between experiment and analytical model without showing clear oscillations. Puga et al. (Puga et al., 2016) studied two different pressure ramps applied on an industrial complex geometry. This works shows qualitatively that the pressure ramp increase leads to higher fluid velocity oscillations and a reduced part quality. Zeng et al. (Zeng et al., 2009) studied the filling of a plate in counter gravity casting for aluminum and for aluminum composite alloys. They also encountered velocity oscillations which are lower when the viscosity of the melt increases. It was shown in the example of an automotive industrial part that the measured filling velocity was lower than the estimation given in Eq-2 due to pressure losses (Hogg et al., 1991). Therefore, previous works showed clearly that mold geometries and pressure ramp can significantly impact the fluid flow. However, the relationship between pressure ramp, mold geometry, melt properties and resulting filling velocity is still unclear.

The present work aims to study the relationship between the imposed gas pressure evolution in the furnace and the induced filling behavior of molds by liquid metal in low pressure sand casting (LPC), both experimentally and numerically. It evaluates in what extent simple hydraulic models can be representative of the filling of a cavity when using LPC, by using adapted simulation hypotheses. This

way, numerical experiments can be performed to define filling rules according to mold geometries in LPC.

2. Filling characterization methods

2.1. Filling experiment

Around $170kg$ of commercial aluminum 13% silicon alloy was melted in electrical low-pressure Kurtz furnace and maintained at 750°C $\pm$ 5°C. A cross-section view of the whole LPC system is shown in Figure 1. The crucible diameter ϕ_f is $545\ mm$, the tube length h_{tube} is $953\ mm$, the tube internal diameter ϕi_{tube} is $70\ mm$ and the tube external diameter ϕe_{tube} is $100\ mm$. The furan resin bonded molds placed at the top of the rising tube were designed and printed using an Exone S-print 3D printer. They were 400 mm in height and cylindrical in shape with a sudden section change of a defined ratio R. During the filling, the pressure ramp was mastered in the low-pressure machine by a pressure regulation system and the air pressure in the furnace was monitored using a pressure sensor. The pressure ramps range admissible by the system is 1 to 30 mbar/s. The cross sections are defined as: $S_f = \frac{\Pi}{4}(\phi_f^2 - \phi e_{tube}^2)$, $S_t = \frac{\Pi}{4}\phi i_{tube}^2$ and $S_c = \frac{\Pi}{4}\phi_c^2$.

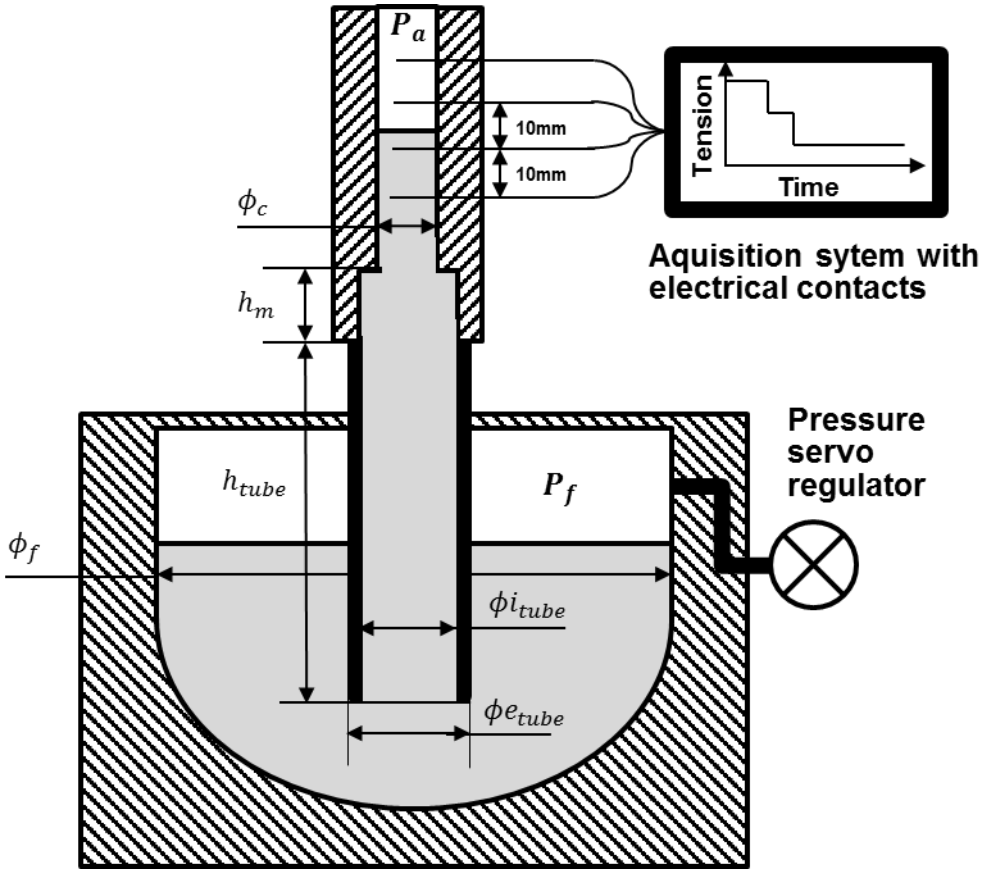

Figure 1 : Vertical cross section view of the Low-pressure casting system and instrumented sand mold

A typical graph of the pressurizing ramp during filling in LPC process is presented in Figure 2. The set pressure evolution has to be distinguished from the actual measured pressure evolution as the pressure regulating system induces some discrepancies. The set pressure evolution corresponds to the set data of the LPC machine when the actual pressure evolution is recorded during each experiment with a pressure uncertainty of 1 mbar, comparable to the 3 mbar precision encountered by Li et al. (LI et al., 2008).

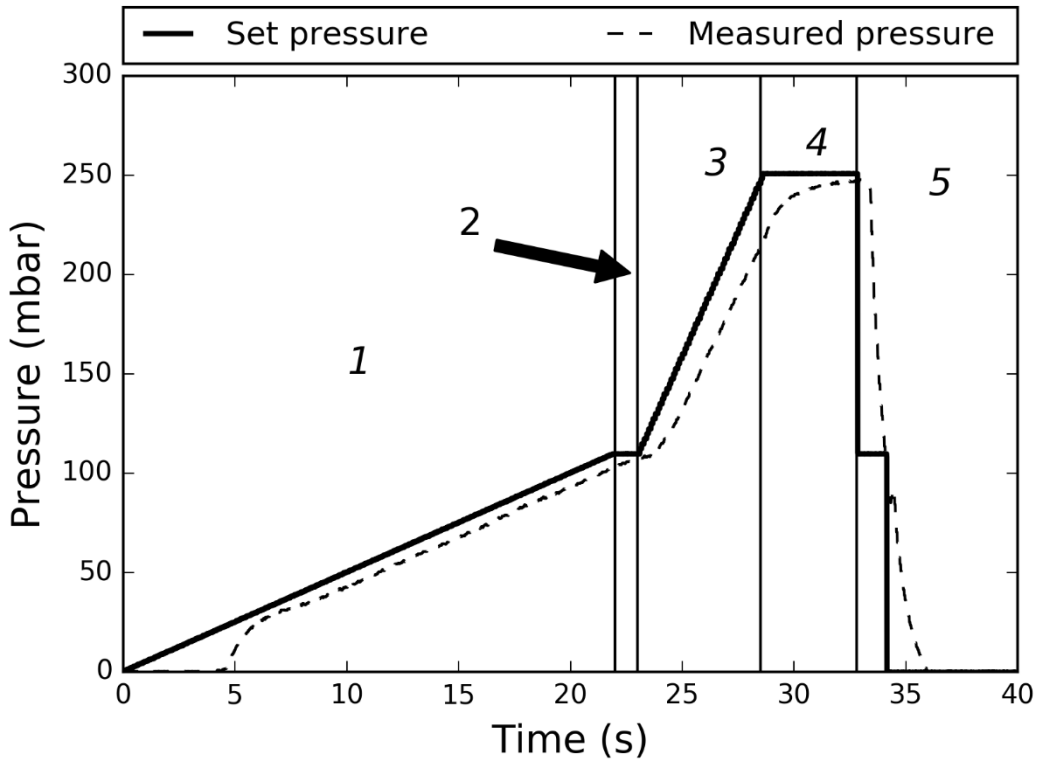

Figure 2 : Typical set and measured pressure time evolutions, for R=1 and $\dot{P}_f = 25\ mbar/s$

The set pressure evolution can be divided into five typical stages. The first stage is the filling of the bottom part of the rising tube with a ramp equal to $5\ mbar.s^{-1}$, until a fixed pre-pressure value. This first stage is identical in all the experiments. Stage II is the stabilization at the pre-pressure value for one second. Then during stage III, the top of the tube and the mold are filled at the filling pressure ramp called here "set pressure ramp" $\dot{\mathrm{P}}_{\mathrm{f}}$. To avoid any mold overflow, the pressure is then stabilized for 4 seconds in stage IV before pressure release in stage V. The experimental pressure evolution can be compared with the set pressure evolution by analyzing Figure 2. The actual pressure evolution is globally delayed and the pressure ramp is progressively slowed down by servo regulator until reaching the final set value.

Two types of experiments were realized. In the first type of experiment, the sand molds are vertical tubes with a constant inner diameter which is equal to the rising tube diameter. Therefore, no section restriction is made and the restriction factor $R = \frac{Sc}{St} = \left(\frac{\phi_c}{\phi i_{tube}}\right)^2$ is equal to 1. In the second group of experiments, the cylindrical molds are designed with a sudden section restriction at $h_m = 100\ mm$ from the bottom of the mold. The four geometries studied are presented in Table .

	Group 1	Group 2		
Section restriction factor R (-)	1	0.5	0.24	0.125
Shape				

Table 1: Samples geometries of the sand molds used in LPC filling experiments at different pressure ramps

For each experiment performed in this study, the rising of the horizontal free surface in the mold was tracked using electrical contacts. It consisted on 1 mm steel rod, inserted until the center of the cylinders at every 10 mm in height. The contact position precision was $\pm$ 2 mm. Each contact was connected to the electrical circuit. During filling, an initial output tension of 11 V was gradually reduced by 0.05 V steps by the electrical circuit when the metal reached a contact. The measurement of the output tension versus time was performed by National Instrument data acquisition at a frequency of 100 Hz.

2.2. Filling simulation

Computational modeling of the filling processes was performed using the commercial software ANSYS Fluent®. The finite volume model associated with free surface volume of fluid modelling (VOF) are described in detail in Fluent theory guide (ANSYS Inc., 2013). The metal was considered as a Newtonian fluid with a constant cinematic viscosity of $0.00113\ kg.m^{-1}.s^{-1}$ and a density of $2495\ kg.m^{-3}$ (Kund and Dutta, 2015). The same assumption was made for the air above the metal in the furnace with a viscosity of $0.0001\ kg.m^{-1}.s^{-1}$ and a density of $1.442\ kg.m^{-3}$ (from Ansys Fluent 16.1 database). To reduce simulation times, the study was performed using a 2D axisymmetric model. To validate the convergence of the computations on the tube case, three different meshes with a mean size of 2 mm, 1 mm and 0.5 mm squared elements were considered. The 1 mm mesh was used in the presented results. The studied geometry being axisymmetric, only one half of the 2D system was computed.

To rate the effect of each LPC system element (i.e. mold, rising tube and furnace) on the observed filling, different geometries were numerically studied from the most simplified case to the most complete one. Figure 3 shows the different studied geometries. In “case A”, only the mold is taken into account (Figure3-(a)). In “Case B” the tube is additionally considered (Figure 3-(b)). Finally in “Case C”, the mold, the rising tube and the metal in the crucible are taken into account (Figure 3-(c)).

In “Case A”, the considered geometry was only the mold, as shown in Figure 3-a. The system was initially fully filled with air and a metal pressure boundary condition was applied on the bottom surface, inducing the rising of the metal in the mold. The pressure boundary condition was a pressure ramp as set in the experiment. The imposed atmospheric pressure on the top surface of the mold permitted the air to escape during metal rising. In the other surfaces of the system, no mass exchange was allowed and a zero-fluid velocity was applied as a boundary condition.

In ”Case B”, illustrated in Figure 3-b, the system geometry was modified to consider both the mold and the total length of the rising tube. The initial and boundary conditions remain unchanged, only the metal volume at the time of section restriction will be higher.

In ”Case C”, the whole LPC system including furnace, metal and the air above it in the crucible were additionally simulated as can be seen in Figure 3-c. The pressure inlet boundary condition was then applied to the air. This case was therefore the most complete studied model of the actual LPC system.

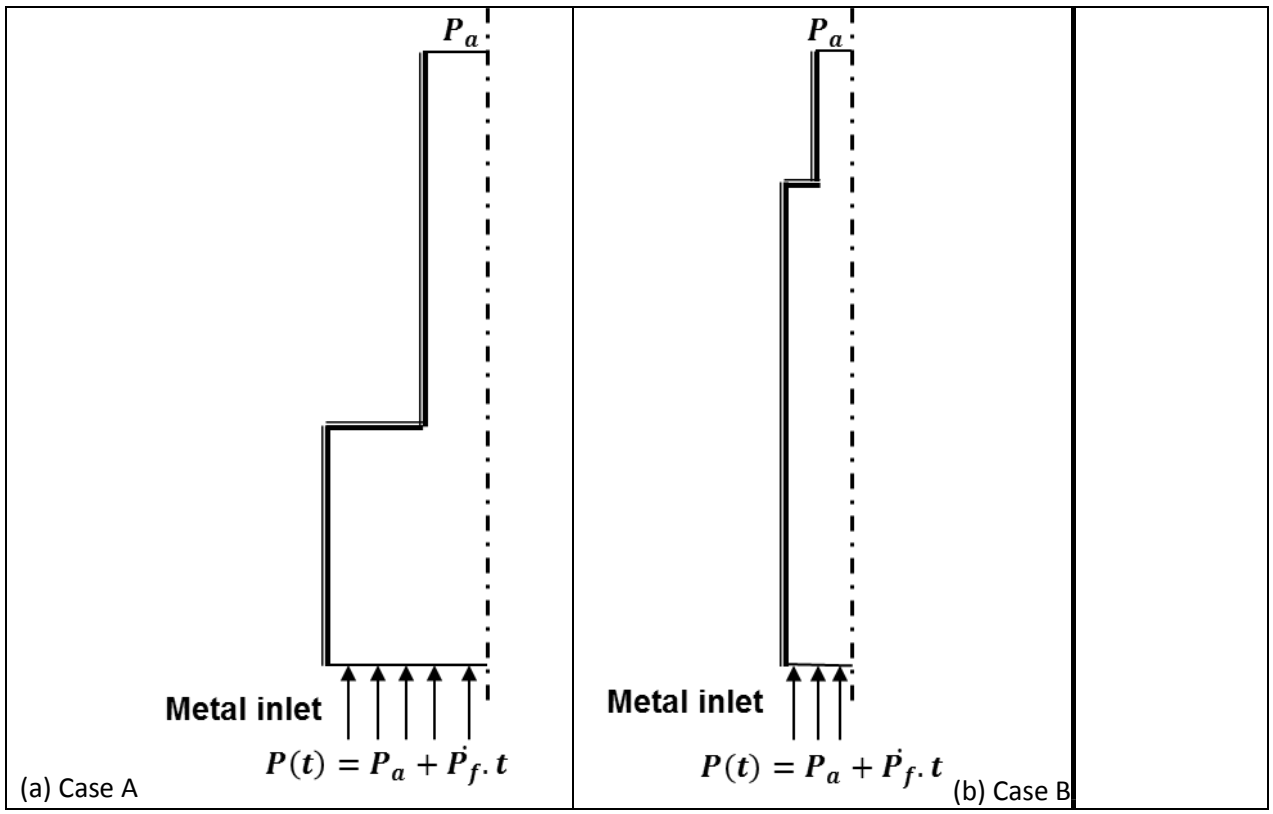

(a) Case A (b) Case B

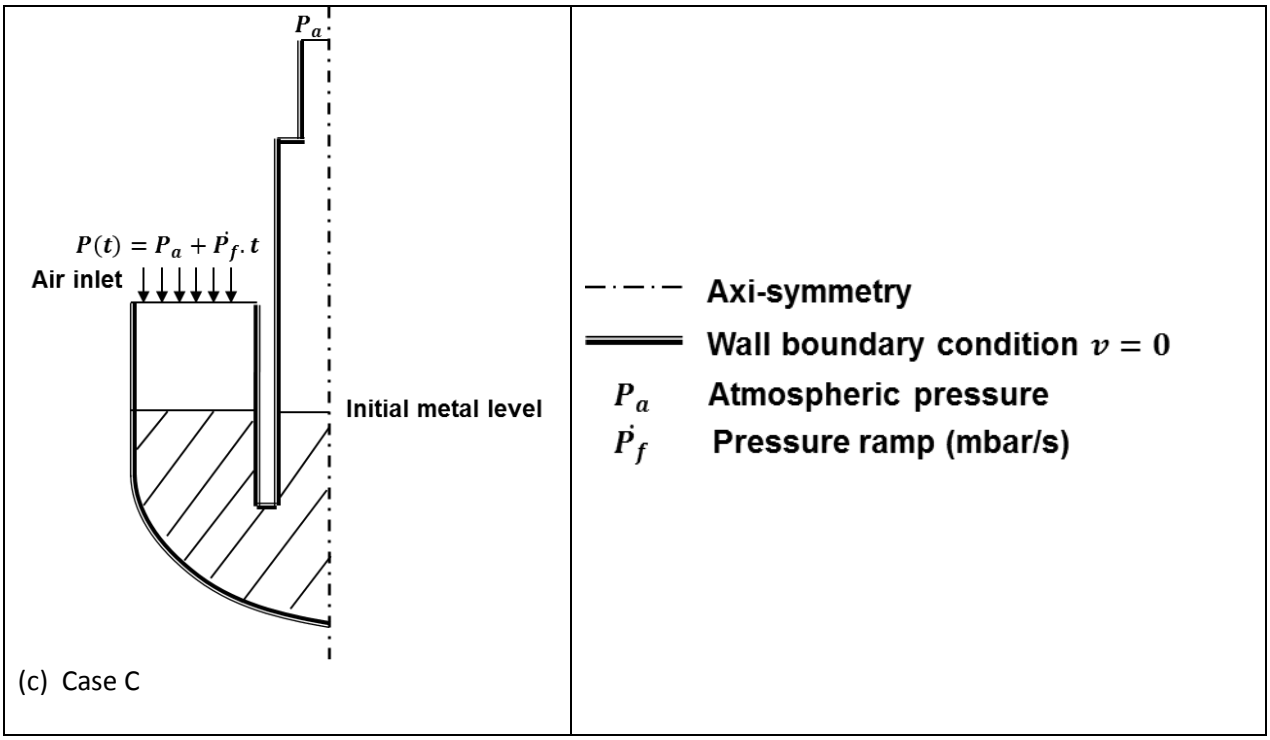

Figure 3 : Boundary and initial conditions for the three studied 2D axi-symmetric model geometries (a) mold, (b) mold and rising tube and (c) mold, rising tube, furnace metal and air

Figure 4 presents the methodology used to extract the simulated metal height to be compared to experimental ones. The metal height was extracted at the center of the axisymmetric model at each time step. As VOF free surface modeling considers a volume fraction evolution in cells which has not a rough slope, the interface between metal and air is gradual. The metal height corresponding to a metal volume fraction of 0.5 was chosen to represent the interface height. For each time step, this interface height was extracted considering a linear interpolation of volume fraction. Then, the metal height was extracted function of the time at each time step.

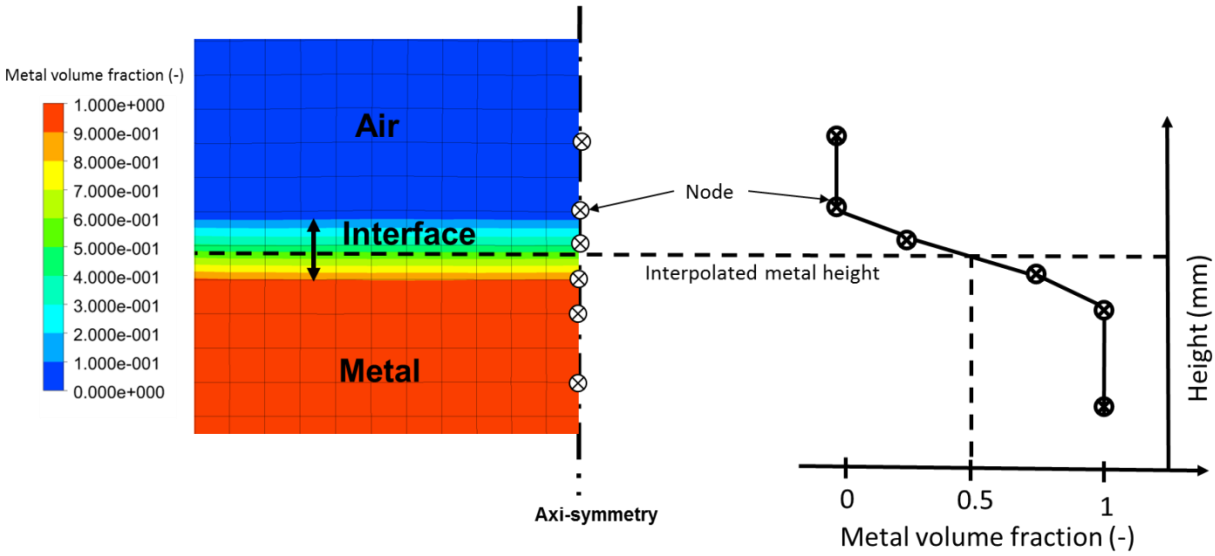

Figure 4 : Definition of simulated metal height at a given time step: (a) 2D visualization of the simulated metal front in the mold cavity and (b) vertical profile of metal volume fraction along the symmetry axis

3. Results

3.1. Experimental results

3.1.1. Mold filling behavior without section restriction (R=1)

The alloy temperature measurements obtained by thermocouples embedded in the molds showed for all the experiments a temperature between 750°C (at the bottom of the mold with the highest filling speed) and 650°C (at the top of the mold with the slowest filling speed). This temperature range -far from the liquidus- allows the assumption of a low variation of density.

The experimental setup permitted to extract the evolution with time of the metal front position in the mold cavity with the same diameter as the rising tube internal diameter. Those positions are then compared with the calculated positions using the measured air pressure in the furnace and the Pascal principle (Eq-1). This comparison, given for R=1 and $\dot{P}_f = 25\ \mathrm{mbar/s}$ in Figure 5, shows a good correlation with the metal height position.

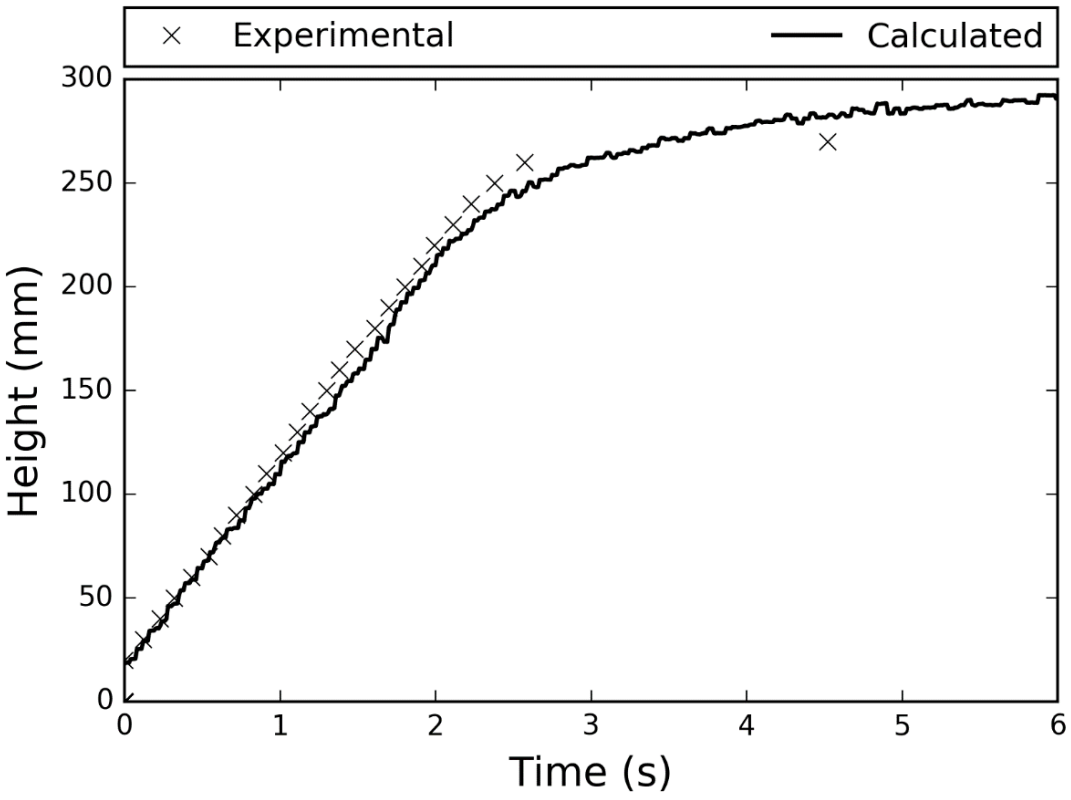

Figure 5 : Calculated and measured position of metal front for R=1 and $\dot{P}_f$ =25 mbar/s, obtained experimentally and by calculation using Pascal principle

For each sample, a linear regression was made on the steady state pressure evolution during stage III of the filling for each of the 11 experiments cast at 5, 15 and 25 mbar/s set pressure ramps. Similarly, a linear regression was made on the steady state part of the height versus time curve giving the average velocity of the metal front. Then, the average velocity was plotted versus the average pressure ramp as shown in Figure 6. This graph shows a linear relationship between filling velocity and the pressure ramp. The highest ramps lead to a higher dispersion. It might be due to the lower accuracy of pressure regulator system at higher pressure ramps.

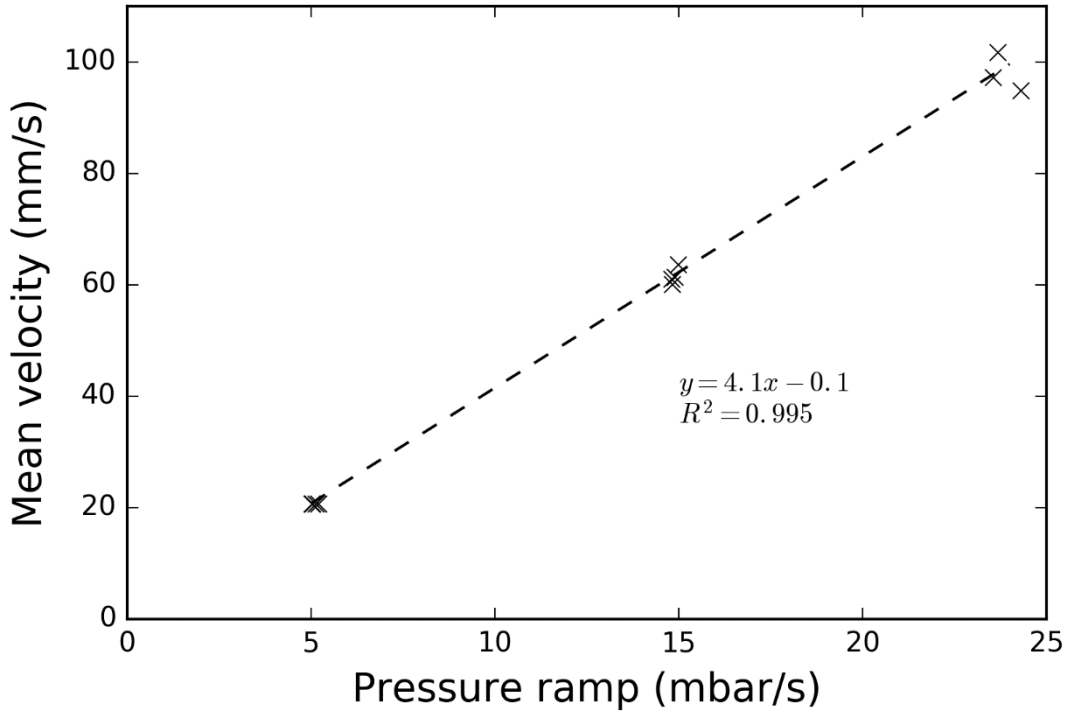

Figure 6 : Experimental average metal front velocity versus average measured pressure ramp in R=1 molds, obtained for 11 filling experiments

Using equation 3 with a restriction ratio of 1, the pressure ramp and the rising velocity can be linearly linked to the alloy density and furnace geometry:

$$v_t = \frac{\mathbf{1}}{\boldsymbol{\rho} g \left(1 + \frac{S_t}{S_f}\right)} \dot{\boldsymbol{P}}_{\boldsymbol{f}} \qquad \text{(Eq-4)}$$

If the furnace geometry is easily characterized ($\alpha = \frac{St}{Sf} = 0.017$), the alloy density is not precisely known as its temperature evolves in the system during filling. However, thanks to the measures presented in Figure 6, the ratio $\frac{v_t}{\dot{\boldsymbol{P}}_{\boldsymbol{f}}}$ can be approximated as a constant: $\frac{v_t}{\dot{\boldsymbol{P}}_{\boldsymbol{f}}} = 4.1\ mm.mbar^{-1}$. Therefore, a density of $2445\ kg.m^{-3}$ is obtained. This value is in the same order of magnitude than the value of $2495\ kg.m^{-3}$ proposed before (Kund and Dutta, 2015). It confirmed that a mean value of density can be used to estimate a mean velocity with equation 3 during filling without section change. Thus, hypothesis of non-viscous fluid and steady state flow can be applied to link height, velocity and pressure ramp when no restriction is present during mold filling. Therefore, once the

velocity range permitting to avoid both misrun and oxidization is chosen, the associated pressure ramp range can be calculated using Eq-4. Considering the typical value of 0.5 m/s as an upper velocity limit, the associated upper limit pressure ramp is 122 mbar/s. This value, well above the machine limit (30 mbar/s), indicates that the filling should not induce oxide film defects in parts when no restriction is present.

3.1.2. Mold filling behavior with section restriction (R<1)

The effect of a section restriction on filling behavior was studied. The three section restriction factors (0.5, 0.24 and 0.125) were tested at five set pressure ramps (5, 10, 15, 20, 25). For each experiment, the actual furnace pressure was measured. It was observed to be similar to the measured pressure when no section restriction was present (Figure 2). It indicates that restriction does not change significantly the gas pressure into the furnace. Then, the metal height versus time curves were analyzed. Figure 7 presents the metal height evolution for the R=0.125 molds. The first stage below the section change shows a steady state filling as for R=1 molds. Above the restriction (at $h_m = 100\ mm$), the metal does not rise linearly anymore. The velocity increases and an oscillating phenomenon starts. Therefore, an over-height of the metal front can be observed comparatively to molds without section restriction.

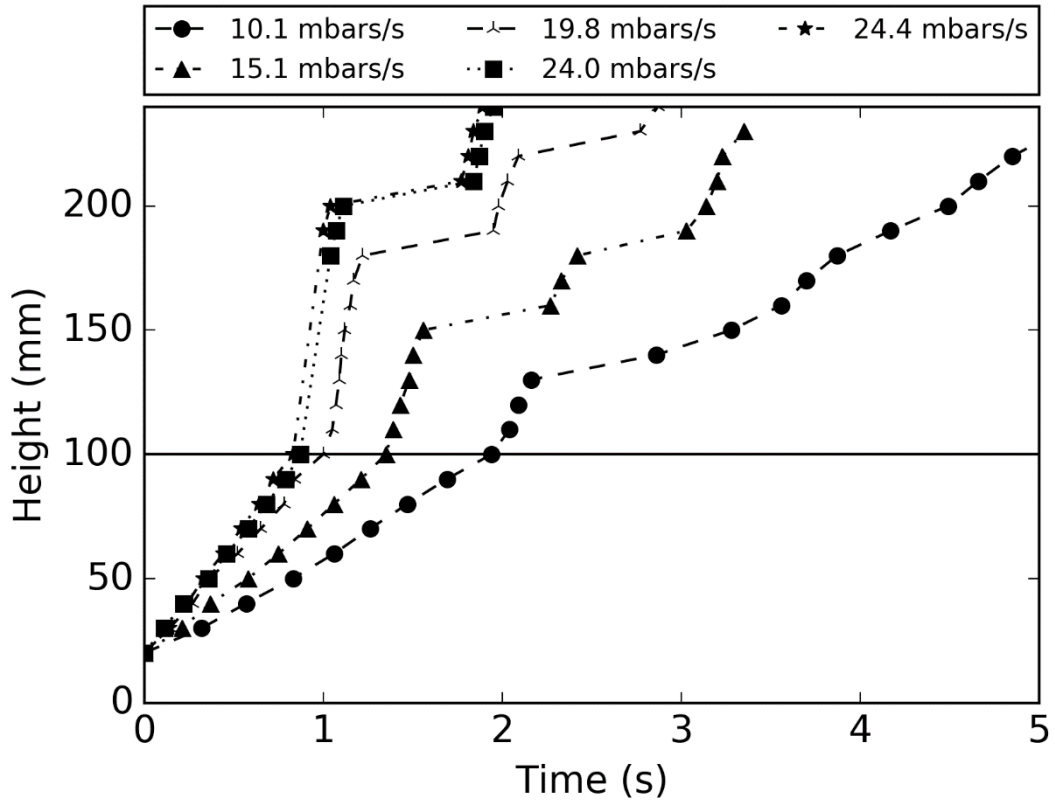

Figure 7 : Measured position of metal height in R=0.125 molds with various measured pressure ramps

To quantify this over-height, the curves were split into two parts: before restriction and after restriction. First part of the curve (i.e. from 20 mm to 100 mm) was fitted with a linear function. This fitted function was then extrapolated to the second part of the curve (i.e. from 100 mm to the top of the mold). This extrapolated function was subtracted to the experimental curve to obtain the effect of section change. The maximum value of this function was extracted and chosen to represent the maximum over-height. For each restriction ratio, this over-height was plotted function of the measured pressure ramp in Figure 8 (a,b,c).

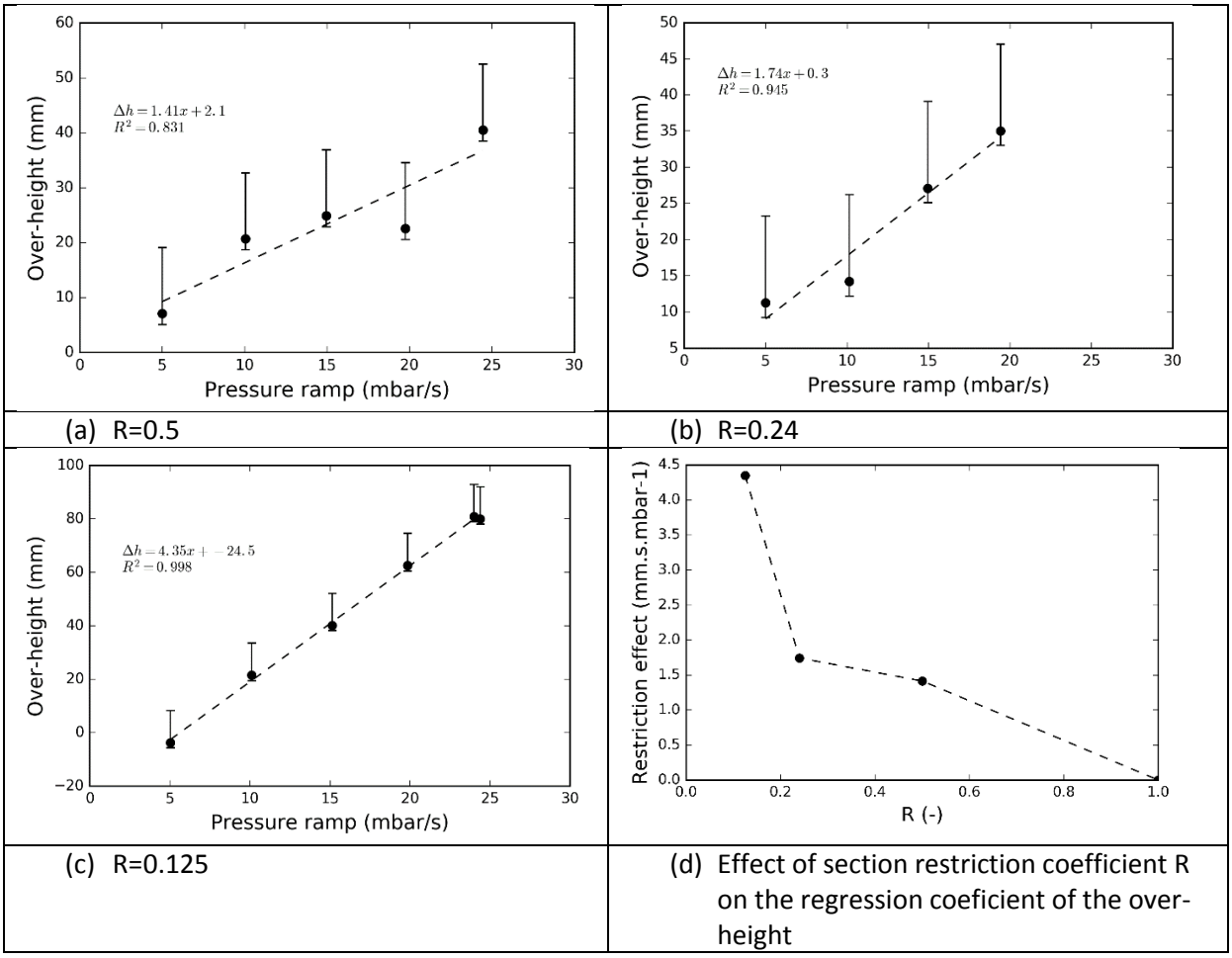

Figure 8 : Maximal measured over height versus measured pressure ramp for the three studied restrictions factors - experimental measurements in dots (●) and interpolated tendency in dashed line (- -)

The lower error bar represents the contact imprecision (2 mm). The upper error bar represents the spacing between two contacts (10 mm) plus the uncertainty of position (2 mm). Indeed, the metal over-height was between the last-reached contact and below the next one (which was not touched yet). As expected, the over-height increases with the increasing of the pressure ramp. A linear regression for each graph shows that the over-height is proportional to pressure ramp. The regression slope for each restriction factor was then plotted function of restriction ratio R in Figure 8-(d). Without restriction, there is no over-height; therefore the impact is set to zero. Thus, the evolution of the over-height with restriction ratio R is not linear. It increases slightly when R decreases from 1 to 0.5. Then the over-height remains relatively stable from 0.5 to 0.24 and it rises for R value below 0.24.

Figure 8-(c) shows a maximum over-height close to 100 mm for R0.125 and 25 mbar/s. Assuming a typical industrial mold height of 400 mm, this over-height corresponds to 25% of the total part height. In practice, this over-height can even lead to overflowing if the mold design is not well adapted to this effect.

Experimental curves were also treated to extract maximum velocities reached during the first wave after section restriction. This velocity was extracted by taking the mean value between two successive experimental contacts. Figure 9 presents the ratio of this measured velocity and the theoretical velocity from equation 3 without restriction for the different experimental cases.

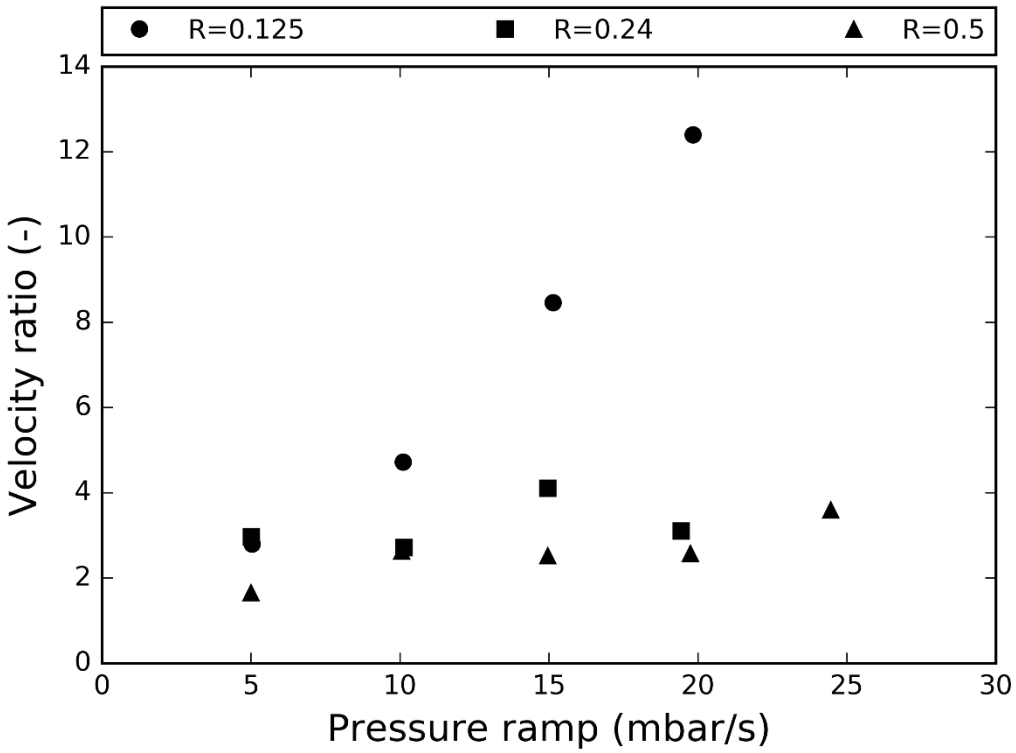

Figure 9 : Ratio of maximum measured metal front velocity and theoretical steady state velocity versus measured pressure ramp

For R=0.24 and R=0.5 restrictions, the maximum velocity ratio increase slightly with the pressure ramp. However, this ratio is significant and remains at a factor close to 3. When the restriction ratio is 0.125, the velocity ratio increasing is clearly linked to the pressure ramp. Velocity can be multiplied by more than a factor ten due to restriction. Actually, in the most critical cases (R=0.125 and 25 mbar/s), acceleration was so high that it could not be measured. Indeed, as the contact spacing is 10 mm and acquisition frequency is 100 Hz, the maximum measurable velocity is 1m/s. Thus, for R=0.125 ratio and 25 mbar/s, the maximum velocity exceeds this value. For the cases with a ratio R<0.125 and $\dot{P}_f$>15 mbar/s, the maximum measured velocity exceeds 0.5 m/s. Therefore, the filling might create oxide film defects in parts even if mean fluid velocity calculated with equations-3 is well below this critical velocity limit.

3.2. Simulation results

One experiment was used as a reference to compare the measured and the numerically predicted fluid flow during LPC filling. In the considered experiment, the restriction factor was $R = 0.125$ and the set pressure ramp was $\dot{P}_f = 15\ mbar/s$. To understand the origin of the oscillations, the experimental and numerical metal height evolutions can be compared. The evolution of the metal heights with time is given in Figure 10.

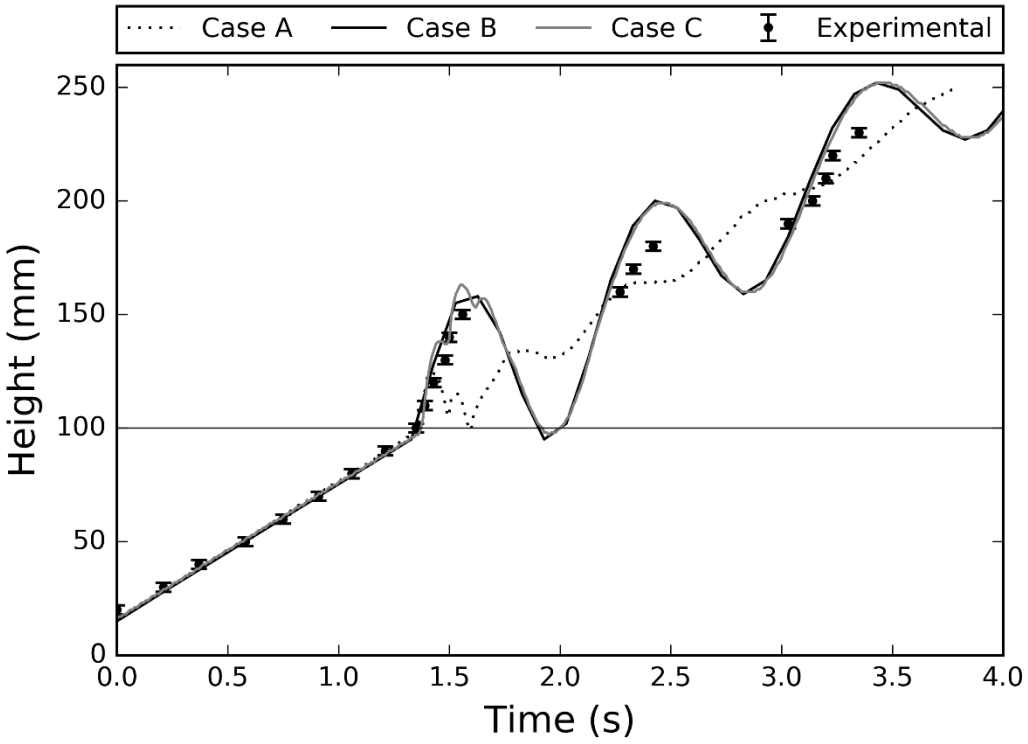

Figure 10 : Comparison of experimental and simulated metal height in the mold versus time

The experimental points are presented with $\pm\ 2mm$ error bars corresponding to the position uncertainty of the contacts. They show the linear rise before restriction. Then, an acceleration of flow is visible at the early instant until a maximum over-height. After that, metal starts to oscillate in height until the end of the filling. All the simulated cases show a good correlation with experiment before the restriction. After the restriction, their behaviors are different. For the simulation of the mold only ("Case A") a minor over-height is observed. Then, oscillating phenomenon is visible but its amplitude is much lower than measured experimentally. For the simulation of the mold and the tube ("Case B") the over-height observed is slightly higher than in the experiment. Then the oscillations fit globally the experimental ones. It reveals that section restriction induces a back flow after restriction. Thus, metal drops below 100mm and pass through the section restriction again. The simulated curve of the whole furnace simulation ("Case C") shows the same tendency as "Case B". However, some little variation can be observed at the top of the over-height.

Simulation showed a complex phenomenon of air bubbles appearing at the restriction, as illustrated in Figure 11. As the model does not simulate the permeability of the sand mold, air bubbles are confined in the liquid. Therefore, it might be responsible of the small measured variations in height in

the simulation “Case C”. Those bubbles create disturbance of the metal front and might lead in real cases to porosities in the cast part. It suggests to design mold geometries to avoid sharp horizontal section restriction, but to prefer continuously varying sections instead. It might enable the air to escape before the metal front arrival.

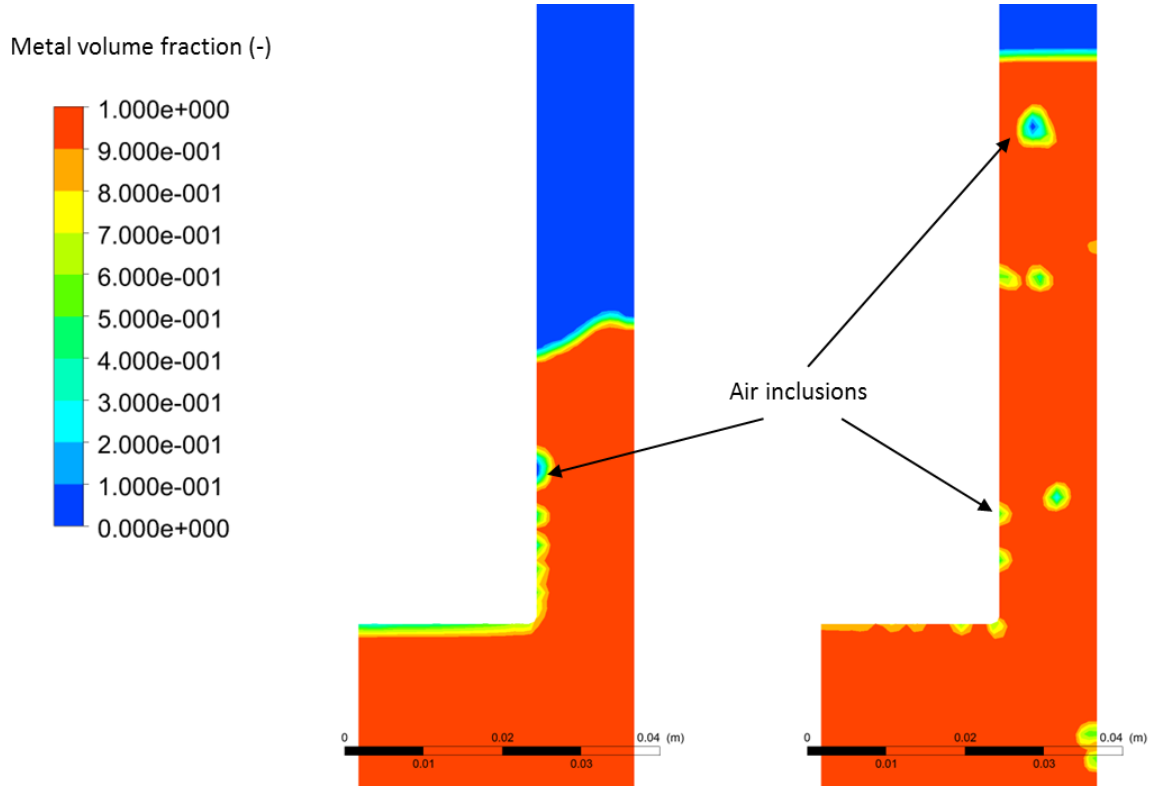

Figure 11 : Observation of simulated air pockets entrapped in the metal at two instants after the section restriction in “Case C”

Considering the numerical and expefigrimental mold filling, the results of “Case A”, where only the mold is considered for the simulation, is not representative. The representability of the two other cases shows that metal volume of the furnace and tube are inducing the oscillating phenomenon due to their dynamic effect. The comparison between “Case B” and “Case C” indicates that the major part of this effect comes from the tube.

4. Discussion

By comparing experimental and analytical filling flow behavior in LPC, it has been shown that without any section change, an average velocity function of pressure ramp and furnace dimensions (given in Eq-3) is representative of the actual metal flow. In this case, the hypotheses of a steady state without pressure losses and an incompressible, irrotational and non-viscous fluid are a good approximation. Then, when a section restriction is considered, oscillations are induced. The intensity of these oscillations was principally characterized by the generated maximum over-height. It was shown

experimentally that this over-height is proportional to the pressure ramp (Figure 8 –(a,b,c)) and exhibits a nonlinear variation with section restriction factor (Figure 8 – d). As the pressure evolution in the furnace remains linear, the oscillations should originate in the dynamic effects of the metal. More precisely, the presented simulations suggest that the main origin of the oscillations is the inertia of the metal in the rising tube. In order to validate this hypothesis, we propose in the following an analytical model to forecast the oscillations intensity as a function of process parameters and geometry.

First of all, we can determine the metal velocity in the different parts of the system. Only the mold and the tube are considered in the following according to simulation results. Assuming that the fluid is non-viscous and incompressible, its velocity in the mold cavity v_c is linked to its velocity in the tube v_t by the mass conservation:

$v_c = \frac{St}{Sc} v_t$ (Eq-5)

Moreover, rewriting Eq-3 by introducing the surfaces ratio $R = \frac{s_c}{s_t}$ and $\alpha = \frac{S_t}{S_f}$, Eq-6 gives the fluid velocity in the tube in steady state:

$v_t = (\frac{\dot{P_f}}{\rho g})(\frac{R}{1+R.\alpha})$ (Eq-6)

Considering a ramp of $15\ mbar.s^{-1}$, the velocities of the metal in the rising tube and in the mold cavity are given depending on the section restriction factor R in Figure 12.

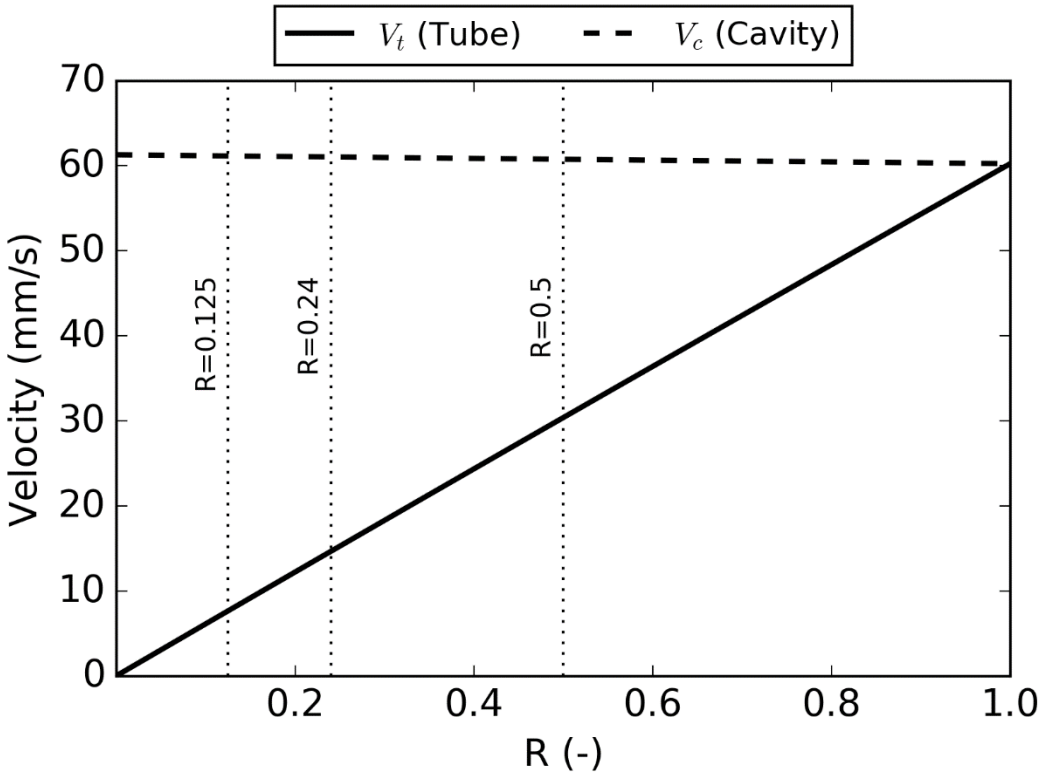

Figure 12 : Theoretical steady state velocities in the rising tube and in the mold cavity for $\dot{P}_f$ = 15 mbar/s as a function of the restriction factor R

If we consider a transition from a steady state with R=1 (i.e. no section change) to a steady state with R=0.125, we see a relative stability of the theoretical metal front velocity v_c (respectively $60.2\ mm.s^{-1}$ and $61.3\ mm.s^{-1}$). However, due to mass conservation, the velocity in the tube is divided by a factor close to $\frac{1}{R} = 8$; it decreases from $60.2\ mm.s^{-1}$ before the section restriction to $7.6\ mm.s^{-1}$ after the section restriction. It clearly appears that the metal velocity reduction in the tube cannot be instantaneous when the metal reaches the section restriction height and the metal kinetic energy has to be transformed. Considering that the system is the metal in the tube when reaching the section restriction height, the kinetic energy of the metal is given by:

$$E_c = \frac{1}{2}\,.\rho.S_t.h_t.v_t^2 \quad \text{(Eq-7)}$$

Where h_t=1.053m is the height of the tube ($h_{tube} = 0.953\ m$) plus the height in the mold below the section change ($h_m = 0.1\ m$). At the exact instant of the restriction, a velocity discontinuity appears, giving two values of v_t . v_{t-} is the tube velocity just before the restriction and to R=1. v_{t+} is the theoretical steady state tube velocity just after the restriction corresponding to a value of R<1. Between these two theoretical states, the kinetic energy difference is:

$$E_{c-} - E_{c+} = \frac{S_t.h_t.\dot{P_f}^2}{2\rho g^2}\left[\left(\frac{1}{1+\alpha}\right)^2 - \left(\frac{R}{1+R\alpha}\right)^2\right] \quad \text{(Eq-8)}$$

This excess of energy could be compensated by pressure losses in the restriction or transformed into potential energy through an over-height. Assuming that the metal is a perfect fluid, the excess energy would be counterbalanced by the potential energy of an over-height h in the restriction:

$E_p = \frac{1}{2}\rho g R.S_t h^2$ (Eq-9)

Then, by combining Eq-8 and Eq-9:

$\frac{1}{2}\rho g R.S_t h^2 = \frac{S_t.h_t.\dot{P_f}^2}{2\rho g^2}\left[\left(\frac{1}{1+\alpha}\right)^2 - \left(\frac{R}{1+R\alpha}\right)^2\right]$ (Eq-10)

By rearranging the terms, the value of the over-height h can be expressed as a function of the pressure ramp $\dot{P}_f$, a constant $C = \frac{\sqrt{h_t}}{\rho.g^{\frac{3}{2}}}$ and a function of the restriction factor $\gamma(R) = \sqrt{\frac{\left(\frac{1}{1+\alpha}\right)^2 - \left(\frac{R}{1+R\alpha}\right)^2}{R}}$:

$h = \dot{P_f}.C.\gamma(R)$ (Eq-11)

Using this equation, the calculated over-height is plotted as a function of pressure ramp and compared to experimental results for three restriction factor values in Figure 13 (a,b,c). Moreover, in order to illustrate the effect of the R ratio in the over-height, C.γ(R) is plotted in Figure 13-(d):

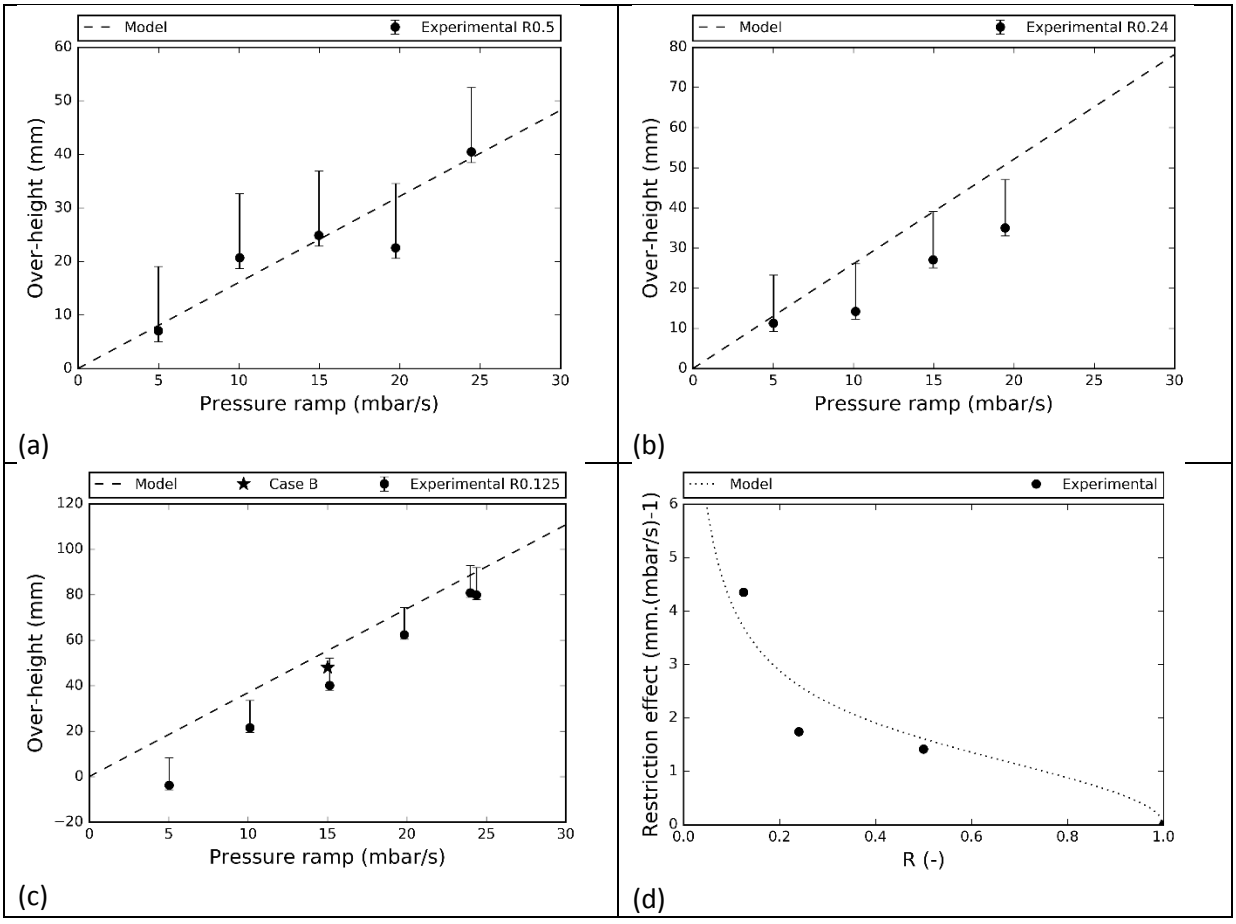

Figure 13 : Calculated and experimental over-height evolution with pressure ramp for (a) R=0.5, (b) R=0.24 and (c) R=0.125, and (d) the proportional coefficient between pressure ramp and over-height C.$\gamma(R)$ as a function of the section restriction factor R

In Figure 13-(a) corresponding to a section restriction factor R=0.5, the model fits well the experimental data; the over-height increases linearly with the pressure ramp. For R=0.24 (Figure 13-(b)), the experimental points tend to be slightly below the model but with the same tendency. In the case R=0.125 (Figure 13-(c)) with a ramp beneath 20 mbar/s, experimental points are relatively below the model. Above 20mbar/s, the over-height is well predicted. The simulation result for "Case B" shown in figure 13 - (c) is also slightly below the analytical model. We can see in Figure 13-(d) that between R=1 and approximatively R=0.3, the model predicts a relatively linear effect of the restriction factor on the maximal over-height. When R<0.3, the effect increases very quickly. Therefore, the non-linear effect of R on the experimentally observed oscillations is qualitatively explained by the γ function non-linearity. As we can see, the best fit between the experiments and the analytical model is obtained for the R=0.5 case. Indeed, the hypotheses of no pressure losses and constant density become less and less applicable when R decreases.

Even though the fluid hypotheses used to develop our analytical model are too basic to precisely quantify the oscillation phenomena, it permits to highlight the influential parameters. Therefore, for a given LPC furnace, two main factors can be extracted: the pressure ramp and the restriction ratio. When the pressure ramp has a linear effect on the maximal over-height, the restriction factor impact, expressed through the γ function, is more ambiguous and should be studied in more detail. However, this analytical model already suggests different ways to optimize the filling. A first guideline is to limit the horizontal section changes in the parts for low-pressure casting. Indeed, the R factor has a huge impact on oscillations generation. This impact is critical for value below 0.125. However, modifying the casted part geometry is not always possible. A second solution to reduce unsteady flow could be the use of a variable pressure ramp. By applying the same methodology as Duan et al. (Duan et al., 2013), the pressure ramp can be reduced just before the section changes and increased again after. However, as the pressure needs to be high enough to prevent misrun, it could be insufficient to prevent oscillations. Another way to limit flow disturbance is to modify the machine dimensions, through the section and height of the rising tube. In the case of an approximately constant part horizontal section, the riser tube section could be adapted to the section of the casted part, keeping R closed to one. Moreover, as the maximal over-height is proportional to the square root of the tube height h_t (Eq-11), it should be kept as small as possible.

The final part quality cannot be directly linked to the maximal over-height. A better indicator could be the maximum velocity. Indeed, these fast accelerations above 0.5 m/s, can be responsible for oxides inclusions. Unfortunately, a simple model linking process parameters and maximal velocity could not be found. However, the simulation model "Case B" with simple hypothesis and relatively low calculation time permits to forecast with good accuracy this phenomenon. Further studies would focus on the relationship between velocity oscillations and defects creation. It would allow to give more precise rules to design parts in low pressure casting by reducing defects creation during filling.

5. Conclusions

The effect of pressure ramp and section restriction factor on mold filling behavior in low pressure casting has been investigated:

- Steady state filling and non-viscous fluid are good first approximations to estimate mean fluid flow velocity in low pressure casting.
- It has been shown that the dynamic effects of the fluid cannot be neglected when the mold section is not constant anymore. The higher the pressure ramp and the section restriction factor are, the more significant the unsteady flow will be. With our LPC machine, it can lead to velocities higher than 0.5 m/s when R<0.125 and $\dot{P}_f$>15 mbar/s.
- In order to minimize the oscillations in LPC, the casted part horizontal section should be as constant as possible.
- Fluid flow simulation software enables to quantitatively predict those dynamic effects considering a viscous newtonian fluid by taking into account both the mold and the rising tube geometries.
- An analytical model was proposed to link the process parameters, the part geometry and the resulting flow disturbances.
- To limit flow disturbances, we also advise to adapt the low-pressure system to the casted part through the tube height and section.

6. Acknowledgements

The authors would like to acknowledge the contribution of colleagues. Thanks are due to J. BOURGEOIS, J. NEGRE and S. BUSSETTA of the Arts et Métiers ParisTech for their precious technical support. S.KHELLADI is thanked for its precious help on fluid flow simulation. The authors also gratefully acknowledge INOVSYS platform for providing the equipment used for this work.

7. Bibliography

ANSYS Inc., 2013. Ansys Fluent Theory Guide.

Campbell, J., 2003. CASTINGS. Elsevier Science.

Duan, J., Maijer, D., Cockcroft, S., Reilly, C., 2013. Development of a 3D Filling Model of Low-Pressure Die-Cast Aluminum Alloy Wheels. Metall. Mater. Trans. A 44, 5304–5315. doi:10.1007/s11661-013-1654-6

Duff, E.S., 1995. Fluid Flow Aspects of Solidification Modelling : Simulation of Low Pressure Die Casting . The University of Queensland.

Edler, F.J., Lagrené, G., Siepe, R., 2006. Thin-walled Mg Structural Parts by a Low-pressure Sand Casting Process, in: Magnesium Alloys and Their Applications. Wiley-VCH Verlag GmbH & Co. KGaA, Weinheim, FRG, pp. 553–557. doi:10.1002/3527607552.ch87

Fan, Z.-T., Ji, S., 2005. Low pressure lost foam process for casting magnesium alloys. Mater. Sci. Technol. 21, 727–734. doi:10.1179/174328405X43199

Flemings, M.C., 1964. Fluidity of metals - techniques for producing ultra-thin section castings. Br. Foundrym. 312–325.

Flemings, M.C., Niiyama, E., Taylor, H.F., 1961. Fluidity of aluminium alloys : An experimental and quantitative evaluation.

Fu, P., Luo, A. a., Jiang, H., Peng, L., Yu, Y., Zhai, C., Sachdev, A.K., 2008. Low-pressure die casting of magnesium alloy AM50: Response to process parameters. J. Mater. Process. Technol. 205, 224–234. doi:10.1016/j.jmatprotec.2007.11.111

Hogg, J.C., Westengen, H., Albright, D.L., 1991. Low pressure sand casting of magnesium alloys, in: Proceedings of the International Symposium on Extraction, Refining and Fabrication of Light Metals, Ottawa, Ontario, Proceedings of Metallurgical Society of Canadian Institute of Mining and Metallurgy. Sahoo, M; Pinfold, P.

Konopka, Z., Zyska, A., Łągiewka, M., Nadolski, M., 2015. The Influence of Pressure Die Casting Parameters on the Castability of AlSi11-SiCp Composites. Arch. Foundry Eng. 15, 29–34. doi:10.1515/afe-2015-0007

Kund, N.K., Dutta, P., 2015. Numerical study of influence of oblique plate length and cooling rate on solidification and macrosegregation of A356 aluminum alloy melt with experimental comparison. J. Taiwan Inst. Chem. Eng. 51, 159–170. doi:10.1016/j.jtice.2015.01.002

Kuo, J.-H., Hsu, F.-L., Hwang, W.-S., 2001. Development of an interactive simulation system for the determination of the pressure–time relationship during the filling in a low pressure casting process. Sci. Technol. Adv. Mater. 2, 131. doi:10.1016/S1468-6996(01)00039-0

Laws, K.J., Gun, B., Ferry, M., 2006. Effect of die-casting parameters on the production of high quality bulk metallic glass samples. Mater. Sci. Eng. A 425, 114–120. doi:10.1016/j.msea.2006.03.037

LI, X., HAO, Q., JIE, W., ZHOU, Y., 2008. Development of pressure control system in counter gravity casting for large thin-walled A357 aluminum alloy components. Trans. Nonferrous Met. Soc. China 18, 847–851. doi:10.1016/S1003-6326(08)60147-8

Liu, S.-G., Cao, F.-Y., Zhao, X.-Y., Jia, Y.-D., Ning, Z.-L., Sun, J.-F., 2015. Characteristics of mold filling and entrainment of oxide film in low pressure casting of A356 alloy. Mater. Sci. Eng. A 626, 159–164. doi:10.1016/j.msea.2014.12.058

Luk, H.W.-K., Darvell, B.W., 1992. Casting system effectiveness— measurement and theory. Dent. Mater. 8, 89–99. doi:10.1016/0109-5641(92)90062-H

Puga, H., Barbosa, J., Azevedo, T., Ribeiro, S., Alves, J.L., 2016. Low pressure sand casting of ultrasonically degassed Al7SiMg alloy: Modelling and experimental validation of mould filling. Mater. Des. 94, 384–391. doi:10.1016/j.matdes.2016.01.059

Runyoro, J., Boutorabi, S.M.A., Campbell, J., 1992. Critical gate velocities for film-forming casting alloys: a basis for process specification. AFS Trans. 100, 225–234.

Sadayappan, M., Thomson, J.P., Sahoo, M., 2006. Casting Fluidity of Magnesium Alloy AZ91 in Gravity and Low Pressure Casting. AFS Trans. 747–753.

Sanitas, A., Coniglio, N., Bedel, M., El Mansori, M., 2017. Investigating surface roughness of ZE41

magnesium alloy cast by low-pressure sand casting process. Int. J. Adv. Manuf. Technol. doi:10.1007/s00170-017-0283-4

Zeng, J., Gu, P., Zou, Y., Xu, Z., 2009. Simulation of mold filling under counter gravity for A356 alloy and A356/SiCp composite. Mater. Sci. Eng. A 499, 130–133. doi:10.1016/j.msea.2007.11.147